

# Polymer Chemistry

Accepted Manuscript



This is an *Accepted Manuscript*, which has been through the Royal Society of Chemistry peer review process and has been accepted for publication.

*Accepted Manuscripts* are published online shortly after acceptance, before technical editing, formatting and proof reading. Using this free service, authors can make their results available to the community, in citable form, before we publish the edited article. We will replace this *Accepted Manuscript* with the edited and formatted *Advance Article* as soon as it is available.

You can find more information about *Accepted Manuscripts* in the [Information for Authors](#).

Please note that technical editing may introduce minor changes to the text and/or graphics, which may alter content. The journal's standard [Terms & Conditions](#) and the [Ethical guidelines](#) still apply. In no event shall the Royal Society of Chemistry be held responsible for any errors or omissions in this *Accepted Manuscript* or any consequences arising from the use of any information it contains.

Cite this: DOI: 10.1039/c0xx00000x

www.rsc.org/xxxxxx

PAPER

# Tetramethylbithiophene in $\pi$ -Conjugated Alternating Copolymers as Effective Structural Component for the Formation of Spherical Assemblies

Liang Tong,<sup>a</sup> Soh Kushida,<sup>a</sup> Junpei Kuwabara,<sup>a</sup> Takaki Kanbara,<sup>a</sup> Noriyuki Ishii,<sup>b</sup> Akinori Saeki,<sup>c</sup> Shu Seki,<sup>c</sup> Seiichi Furumi<sup>d</sup> and Yohei Yamamoto\*<sup>a</sup>

Received (in XXX, XXX) Xth XXXXXXXXX 20XX, Accepted Xth XXXXXXXXX 20XX

DOI: 10.1039/b000000x

$\pi$ -Conjugated alternating copolymers containing a tetramethylbithiophene unit show a strong tendency to form well-defined, sub- to several-micrometer-sized spheres. The twisted bithiophene unit inhibits interchain stacking and anisotropic crystal growth of these copolymers, leading to the formation of structurally isotropic spheres by means of a slow diffusion of nonsolvent into a solution of the copolymers. These micrometer-sized spheres display extremely long photocarrier lifetimes ( $\sim 10^{-3}$  s) in comparison with cast films from the solutions of the polymers and those of the irregular aggregates ( $< 10^{-6}$  s).

## Introduction

Polymer colloids are utilized in various applications such as catalyst support,<sup>1–4</sup> drug and gene delivery,<sup>5–7</sup> biosensors,<sup>8,9</sup> gas sensors,<sup>10,11</sup> and so forth. In particular, colloids composed of  $\pi$ -conjugated polymers are highly valuable for optical applications such as fluorescence imaging and cellular tracking.<sup>12,13</sup> However,  $\pi$ -conjugated polymers are generally difficult to assemble into well-defined spheres because of their rigid and planar backbones, thus limiting the number of reported examples of  $\pi$ -conjugated polymer spheres.<sup>14–16</sup> Hence, the development of a general methodology for the quantitative formation of colloidal particles from  $\pi$ -conjugated polymers will further advance colloid science toward the application of not only single particles but also colloid assemblies in polymer colloid photonic crystals.<sup>17–19</sup>

In this context, we recently reported that several  $\pi$ -conjugated alternating copolymers having fluorene and thiophene repeating units tend to form well-defined spheres under certain self-assembling conditions.<sup>20</sup> The yielded spheres exhibited extremely long photocarrier lifetimes, possibly because of the suppression of charge recombination. In this Article, we comprehensively study structural factors related to the formation of spherical assemblies from  $\pi$ -conjugated alternating copolymers, and show that the use of tetramethylbithiophene (TMT2) as one of their repeating units results in a strong tendency to form well-defined spheres that are sub- to several-micrometers in diameter. The steric hindrance due to four methyl groups on the bithiophene unit markedly lowers the planarity of the polymer backbone, inhibiting the interchain stacking of the polymers and thus leading to the formation of structurally isotropic spheres. This finding provides a new molecular design strategy toward the realization of photo- and electroluminescent

polymer colloids.

## Results and discussion

### Self-assembly of alternating copolymers

We previously showed that an alternating copolymer **F8T2** comprising dioctylfluorene (F8) and bithiophene (T2) repeating units (Fig. 1) yielded irregular aggregates by the slow diffusion of nonsolvent such as MeOH into a solution of the polymers.<sup>20</sup> Conversely, **F8TMT2**<sup>21</sup> containing F8 and TMT2 repeating units (Fig. 1) quantitatively formed spheres under identical self-assembling conditions.<sup>20</sup> Herein, we investigate the self-assembling behaviors of additional five alternating copolymers, **DOPMT2**, **PTTMT2**, **3,6-CTMT2**, **2,7-CTMT2**, and **DPPTMT2**,<sup>22</sup> in which all polymers possess the TMT2 unit as one of the repeating units, and a different arylene unit as the counterpart: *para*-dioctylphenylene (DOP), phenothiazine (PT),

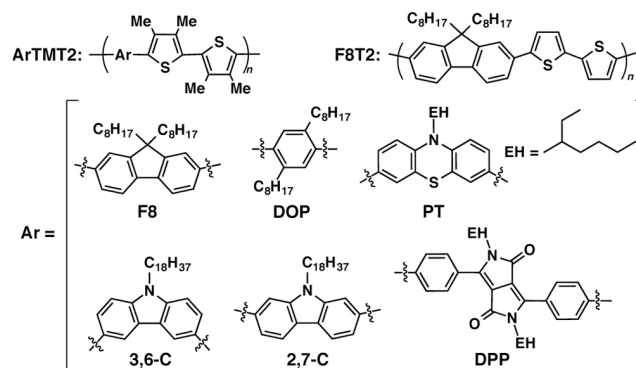
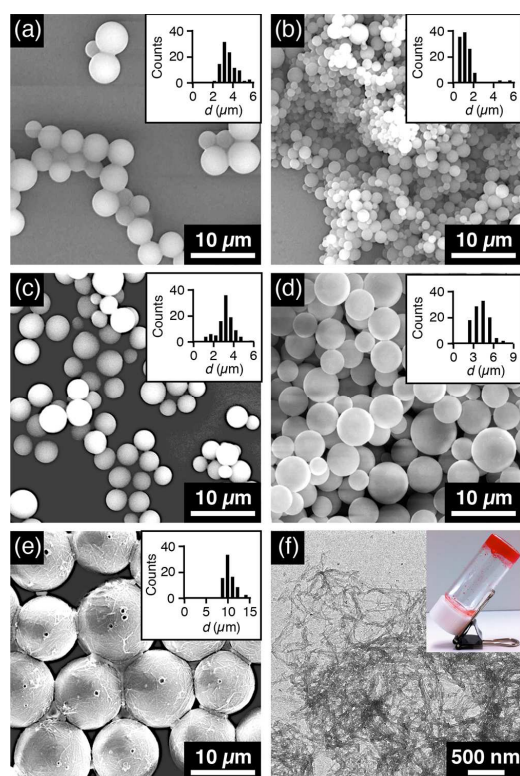


Fig. 1 Molecular structures of seven  $\pi$ -conjugated alternating copolymers.



**Fig. 2** (a–e) SEM micrographs of air-dried  $\text{CHCl}_3/\text{MeOH}$  suspensions of the spherical assemblies of **DOPTMT2** (a), **PTTMT2** (b), **3,6-CTMT2** (c), **2,7-CTMT2** (d), and **DPPTMT2** (e). Insets show histograms of the spheres' diameter. (f) TEM micrograph of an air-dried  $\text{CH}_2\text{Cl}_2/\text{acetone}$  gel of **DPPTMT2**. Inset shows an optical micrograph of the gel.

**Table 1.** Morphologies of the self-assembled precipitates formed from  $\pi$ -conjugated alternating copolymers by a slow diffusion of MeOH vapor into various solutions.<sup>[a]</sup> Numerical values in parentheses indicate the average diameter ( $d_{\text{av}}$ ) and standard deviation ( $\sigma$ ) of the spheres.

	$\text{CHCl}_3$ ( $d_{\text{av}}$ , $\sigma/\mu\text{m}$ )	THF ( $d_{\text{av}}$ , $\sigma/\mu\text{m}$ )	$\text{CH}_2\text{Cl}_2$ ( $d_{\text{av}}$ , $\sigma/\mu\text{m}$ )
<b>F8T2</b> <sup>[b]</sup>	×	×	–
<b>F8TMT2</b> <sup>[b]</sup>	⊙ (2.4, 1.2)	⊙ (1.9, 0.7)	⊙ (2.7, 0.4)
<b>DOPTMT2</b>	⊙ (3.7, 0.8)	⊙ (1.8, 0.7)	×
<b>PTTMT2</b>	⊙ (1.3, 0.4)	△ (1.9, 0.6)	⊙ (1.9, 0.5)
<b>3,6-CTMT2</b>	⊙ (3.2, 0.8)	⊙ (2.4, 1.0)	×
<b>2,7-CTMT2</b>	⊙ (4.3, 1.1)	⊙ (1.7, 0.7)	×
<b>DPPTMT2</b>	△ (11.1, 1.1)	–	×

<sup>[a]</sup> ⊙, well-defined spheres; △, distorted or fused spheres; ×, irregular aggregates; –, low solubility. <sup>[b]</sup> Reference 20.

3,6-carbazole (3,6-C), 2,7-carbazole (2,7-C), and diketopyrrolopyrrole (DPP), respectively. For self-assembly, a 5-mL vial containing a  $\text{CHCl}_3$ ,  $\text{CH}_2\text{Cl}_2$ , or THF solution of the polymers ( $1 \text{ mg mL}^{-1}$ , total amount of 2 mL) was placed in a 50-mL vial containing 5 mL of nonsolvents such as acetone or MeOH. The outer vial was capped and kept in dark at a constant temperature of 25 °C. The nonsolvent vapor gradually diffused into the solution of the polymers to give a suspension after 3 days (Fig. S1†).

Figs. 2a–2e show the scanning electron microscopy (SEM)

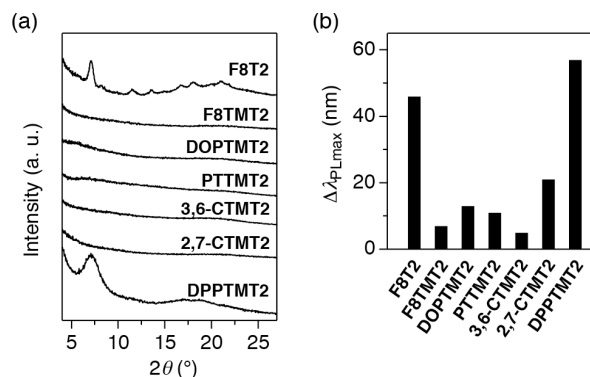


**Fig. 3** (a) Powder XRD patterns of thin films of ill-aggregated **F8T2**, spherical assemblies of **F8TMT2**, **DOPTMT2**, **PTTMT2**, **3,6-CTMT2**, and **2,7-CTMT2**, and self-assembled nanofibers of **DPPTMT2**. (b)  $\Delta\lambda_{\text{PL,max}}$  of the copolymers between solution and self-assembled spheres or aggregates.

images of the air-dried suspension of the polymers with a solvent combination of  $\text{CHCl}_3$  (good solvent) and MeOH (nonsolvent). For **DOPTMT2**, **PTTMT2**, **3,6-CTMT2**, and **2,7-CTMT2**, well-defined spheres were observed with diameters ( $d$ ) ranging from 0.2 to 8.0  $\mu\text{m}$  (Figs. 2a–2d). The average diameter ( $d_{\text{av}}$ ) and standard deviation ( $\sigma$ ) values were dependent on the solubility of the polymers and the solvent combination. Table 1 shows the morphologies of the precipitates afforded from various solutions of the copolymers upon diffusion of the MeOH vapor. Spheres were formed from the  $\text{CHCl}_3$  and THF solutions of the four aforementioned copolymers, while  $\text{CH}_2\text{Cl}_2$  solutions did not always afford spheres (Figs. S2–S5). This is possibly because the precipitation takes place too rapidly. However, the  $\sigma$  values were rather small for rapid precipitation from  $\text{CH}_2\text{Cl}_2$  solution (Table 1). The  $d_{\text{av}}$  and  $\sigma$  values of the obtained spheres are possibly determined by factors such as the mixing rate of good solvent and nonsolvent, and the solubility of the polymers.<sup>20</sup> In addition, slow diffusion of polar nonsolvent is required for spherical assembly, because the hydrophobic polymers tend to assemble while minimizing the contact area with the polar nonsolvents.<sup>20</sup>

In contrast, **DPPTMT2** showed different self-assembly behavior. For the  $\text{CHCl}_3/\text{MeOH}$  solvent combination, spherical assemblies were obtained with an average diameter ( $d_{\text{av}}$ ) of 11.1  $\mu\text{m}$ , which is apparently larger than that formed from other copolymers (Fig. 2e). Furthermore, the surfaces of the spheres were not as smooth as those of the other spheres, appearing to be aggregates of fibers (Fig. S6). In fact, when acetone vapor was diffused into a  $\text{CH}_2\text{Cl}_2$  solution of **DPPTMT2**, a gel formed (Fig. 2f, inset). Transmission electron microscopy (TEM) of the gel, diluted by acetone and ultrasonicated for a short period, displayed thin nanofibers with a width of 10–20 nm (Fig. 2f). Accordingly, the spheres formed from **DPPTMT2** likely consist of aggregates of thin nanofibers.

### Structural characterization of the spheres

X-ray diffraction (XRD) studies of the self-assembled precipitates demonstrate a clear relationship between their morphology and crystallinity. The copolymers of irregularly aggregated **F8T2** and nanofibrous assembly of **DPPTMT2** exhibited diffraction peaks at  $2\theta \sim 7^\circ$  ( $d \sim 12 \text{ \AA}$ ), which is attributed to the periodicity of the lateral arrays of the main chain

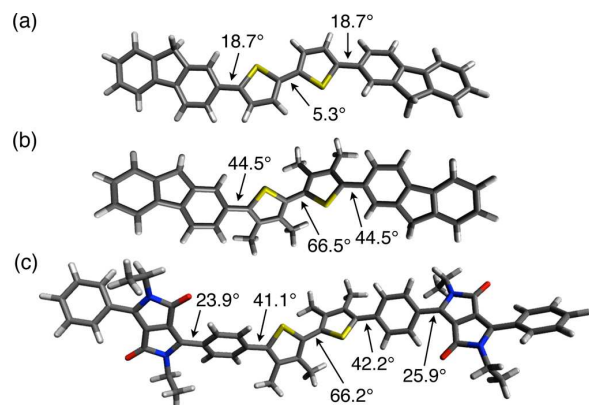


**Fig. 4** Calculated molecular configurations of **F8T2** (a), **F8TMT2** (b) and **DPPTMT2** (c) by DFT calculations. Dihedral angles between the neighboring rings are drawn.

of the polymers (Fig. 3a). In contrast, the other five copolymers with spherical morphologies did not show any particular diffraction peaks in the whole  $2\theta$  region (Fig. 3a), indicating that the spheres are composed of amorphous assembly of the

5 copolymers. Such clear differences were also observed in the photoluminescence (PL) spectra, where a significant red-shift was observed for suspensions of the self-assembled aggregates of **F8T2** and **DPPTMT2** in comparison with their solutions with the

10 PL peak shift,  $\Delta\lambda_{\text{PL,max}}$ , of 46 and 57 nm, respectively (Figs. 3b and S7). Meanwhile, the  $\Delta\lambda_{\text{PL,max}}$  values between the solution and suspension of the spheres for the other five copolymers were comparatively small within the range of 5–21 nm (Figs. 3b and S7), implying that interchain  $\pi$ -electronic interactions are very

15 small in their spherical morphologies. These XRD and PL results indicate that copolymers with low crystallinity tend to form spheres, while those having a high crystallinity rarely form spheres.

According to the density function theory (DFT) calculations,<sup>‡</sup>

20 the dihedral angles between the neighboring  $\pi$ -planes in **F8T2** are less than 20° (Fig. 4a), but those in **F8TMT2** are apparently large (44–67°, Fig. 4b). Such a large torsion in the TMT2 unit possibly inhibits the interchain stacking and anisotropic crystal growth of the polymers, leading to the formation of amorphous spheres with

25 an isotropic geometry. For the other alternating copolymers that form spheres, the similar twisting of the TMT2 unit likely occurs. The only exception is the donor (D)–acceptor (A) copolymer **DPPTMT2**, where a strong interchain D–A interaction possibly takes place,<sup>23,24</sup> resulting in a nanofibrous assembly of polymers,

30 even though the polymer main chain involves a highly twisted TMT2 unit (Fig. 4c). In addition, two phenylene groups attached on both sides of the TMT2 group cause better planarity of the main chain of **DPPTMT2**, which might help interchain stacking of the polymer.

### 35 Photocarrier lifetime studies

The photocarrier half-lifetime ( $\tau_{1/2}$ ) was greatly enhanced when the polymers form spheres. Figs. 5a–5c shows flash-photolysis time-resolved microwave conductivity (FP-TRMC)<sup>25,26</sup> profiles of **DOPTMT2**, **PTTMT2**, and **DPPTMT2** for cast films from their solutions (black) and self-assembled aggregates (red). Upon

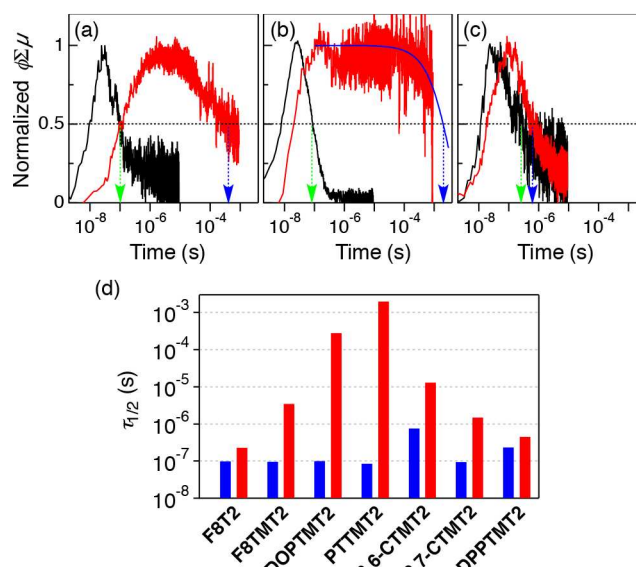


**Fig. 5** (a–c) FP-TRMC profiles of thin films of **DOPTMT2** (a), **PTTMT2** (b) and **DPPTMT2** (c) cast from  $\text{CHCl}_3$  solution (black) and suspensions of self-assembled spheres or aggregates (red). The green and blue arrows indicate  $\tau_{1/2}$  of thin films cast from solution and suspensions of self-assembled spheres or aggregate, respectively. The  $\tau_{1/2}$  value of the self-assembled spheres of **PTTMT2** was determined by a curve fitting of a single-exponential decay of the TRMC signal (blue curve in b). (d) Bar chart of the photocarrier lifetimes ( $\tau_{1/2}$ ) of thin films cast from  $\text{CHCl}_3$  solution (blue) and suspensions of self-assembled spheres or aggregates (red). The  $\tau_{1/2}$  values are defined by the time when the FP-TRMC transient decays down to a half of its maximum value. The data of **F8T2** and **F8TMT2** are referred from ref. 20.

laser flash ( $\lambda_{\text{ex}} = 355$  nm), rise and decay profiles of a TRMC signal, given by  $\phi\Sigma\mu$ , are observed, where  $\phi$  and  $\Sigma\mu$  represent photocarrier generation yield and sum of the mobilities of generated charge carriers, respectively. It is clear that the decay

45 of the TRMC signals for spherically assembled copolymers are quite slow in comparison with that of the films from their solutions or irregular aggregates. For example,  $\tau_{1/2}$  of the spherically assembled **DOPTMT2** is 280  $\mu\text{s}$ , which is more than  $10^3$  times longer than that of the solution-cast film of **DOPTMT2**

50 ( $\sim 0.1$   $\mu\text{s}$ , Fig. 5a). The degree of the enhancement of  $\tau_{1/2}$  is much greater for **PTTMT2** (Fig. 5b), where the ratio of  $\tau_{1/2}$  for the films of the spheres to that for the solution-cast film reaches  $2.3 \times 10^4$  (Table S1). In contrast, **DPPTMT2** do not show such marked enhancement of  $\tau_{1/2}$  between the thin film from its

55 solution and that of nanofibrous assembly (Fig. 5c). The other polymers show the similar tendency that the spherical assembly exhibits at least 15 times longer  $\tau_{1/2}$  values than the solution-cast films, while the irregularly aggregated polymers shows similar  $\tau_{1/2}$  values to the corresponding solution-cast films (Fig. S8 and

60 Table S1).

The elongation of  $\tau_{1/2}$  found in the spheres is likely due to the suppression of bulk charge recombination, facilitated by the isolation of each sphere. In fact, spheres with the smallest diameters, formed from **PTTMT2**, afford the largest  $\tau_{1/2}$  value.

65 The investigation of the detailed elementary steps is ongoing in order to know why the spherical geometry enhanced photocarrier lifetime so markedly.

Noteworthy is that PL quantum yield ( $\phi_{\text{PL}}$ ) is slightly enhanced by the spherical formation. Table S2 lists the absolute  $\phi_{\text{PL}}$  values of the copolymers in the solid state. The spherically assembled samples displayed as well or better  $\phi_{\text{PL}}$  in comparison with cast films from their  $\text{CHCl}_3$  solutions. On the other hand, irregularly assembled samples (**F8T2** and **DPPTMT2**) showed worse  $\phi_{\text{PL}}$  than cast films from their  $\text{CHCl}_3$  solutions.

## Conclusion

We have shown that tetramethylbithiophene is a powerful structural component in the formation of spherical structures, yielding a useful tool for developing strategies for converting  $\pi$ -conjugated polymers into colloidal assemblies. Most copolymers having a tetramethylbithiophene unit form well-defined microspheres quantitatively, except for the case of donor-acceptor copolymer. By the formation of spherical geometry, photocarrier lifetime is extremely elongated, which will be beneficial for utilizing these colloids as optical and optoelectronic materials. The construction of colloidal crystals from  $\pi$ -conjugated polymers will realize new optoelectronic devices such as light-emitting photonic crystals.<sup>27</sup>

## Experimental Section

### Materials

Unless otherwise noted, reagents and solvents were used as received from Aldrich Chemical Co. Ltd and Nakarai Tesque Co., respectively. Alternating copolymers, poly[(9,9-dioctylfluorenyl-2,7-diyl)-*alt*-(bithiophene-2,5'-diyl)] (**F8T2**, number-averaged molecular weight ( $M_n$ ) = 26600, polydispersion index ( $M_w/M_n$ ) = 2.66), poly[(9,9-dioctylfluorenyl-2,7-diyl)-*alt*-(3,3',4,4'-tetramethylbithiophene-2,5'-diyl)] (**F8TMT2**,  $M_n$  = 31800,  $M_w/M_n$  = 2.46), poly[(1,4-dioctylphenyl-2,5-diyl)-*alt*-(3,3',4,4'-tetramethylbithiophene-2,5'-diyl)] (**DOPTMT2**,  $M_n$  = 15000,  $M_w/M_n$  = 1.69), poly[(*N*-(2-ethylhexyl)phenothiazine-3,7-diyl)-*alt*-(3,3',4,4'-tetramethylbithiophene-2,5'-diyl)] (**PTTMT2**,  $M_n$  = 21000,  $M_w/M_n$  = 2.82), poly[(*N*-octadecylcarbazol-3,6-diyl)-*alt*-(3,3',4,4'-tetramethylbithiophene-2,5'-diyl)] (**3,6-CTMT2**,  $M_n$  = 11700,  $M_w/M_n$  = 1.93), poly[(*N*-octadecylcarbazol-2,7-diyl)-*alt*-(3,3',4,4'-tetramethylbithiophene-2,5'-diyl)] (**2,7-CTMT2**,  $M_n$  = 26000,  $M_w/M_n$  = 2.76), and poly[(2,5-bis(2-ethylhexyl)-3,6-bis(phenyl)pyrrolo[3,4-*c*]pyrrole-1,4-dione-4',4''-diyl)-*alt*-(3,3',4,4'-tetramethylbithiophene-2,5'-diyl)] (**DPPTMT2**,  $M_n$  = 18100,  $M_w/M_n$  = 2.35), were synthesized according to the reported procedures.<sup>20–22</sup>

### Measurements

SEM microscopies were performed at 25 °C on a JEOL model JSM-5610 scanning electron microscopy operating at 20 kV. Silicon was used as a substrate and 5-nm of Au was deposited onto the cast films from the suspension of the polymers. TEM microscopy was recorded on a Philips model Tecnai F20 electron microscope operating at 120 kV. Sample dispersions were applied onto a specimen grid covered with a thin carbon support film, which had been hydrophilized by a JEOL model HDT-400 ion bombardment device. Images were recorded on a Gatan slow scan CCD camera (Retractable Multiscan Camera) under low dose conditions. Powder X-ray diffraction patterns were recorded at 298 K on a Rigaku model Miniflex600 X-ray diffractometer with a  $\text{CuK}\alpha$  radiation source (40 kV and 15 mA). Photoluminescence spectra were measured at 25 °C

with a JASCO model FP-6200 spectrofluorometer. Molecular configurations were optimized at the B3LYP/6–31G level DFT calculations with the Gaussian09 program.<sup>‡</sup> FP-TRMC measurements were carried out at 25 °C in air, where the resonant frequency and microwave power were set at ~9.1 GHz and 10 mW, respectively, so that the electric field of the microwave was small enough not to disturb the thermal motion of charge carriers.<sup>28</sup> The charge carriers were photochemically generated using the third-harmonic generation (THG, 355 nm) light pulses from a Spectra Physics model INDI Nd:YAG laser (5–8 ns pulse duration) with incident photon densities of  $9.1 \times 10^{15}$  photons  $\text{cm}^{-2}$ . The TRMC signals, picked up by a diode (rise time < 1 ns), were monitored by a Tektronics model TDS3052B digital oscilloscope. The observed conductivities were converted into normalized values, given by a photocarrier generation yield ( $\phi$ ) multiplied by sum of the charge carrier mobilities ( $\Sigma\mu$ ), according to an equation  $\phi\Sigma\mu = (1/eA I_0 F_{\text{light}})(\Delta P_r/P_r)$ , where  $e$ ,  $A$ ,  $I_0$ ,  $F_{\text{light}}$ ,  $P_r$  and  $\Delta P_r$  denote unit charge of a single electron, sensitivity factor ( $\text{S}^{-1} \text{cm}$ ), incident photon density of excitation laser (photon  $\text{cm}^{-2}$ ), filling factor ( $\text{cm}^{-1}$ ) and reflected microwave power and its change, respectively. The sample films for FP-TRMC measurements were prepared by drop-cast onto quartz plates of the precipitates prepared by vapor diffusion method or  $\text{CHCl}_3$  solutions. Absolute PL quantum yield were measured with Hamamatsu model C9920-02G absolute PL quantum yield measurement system equipped with a Hamamatsu model C10027-01 photonic multichannel analyzer.

## Conflict of interest

The authors declare no competing financial interest.

## Acknowledgments

This work was partly supported by a Grant-in-Aid for Young Scientists A (25708020) from MEXT, Japan, the Industrial Technology Research Grant Program (2011, NEDO, Japan), Cooperative Research Program of "Network Joint Research Center for Materials and Devices", Asahi Glass Foundation, and Tokuyama Science Foundation.

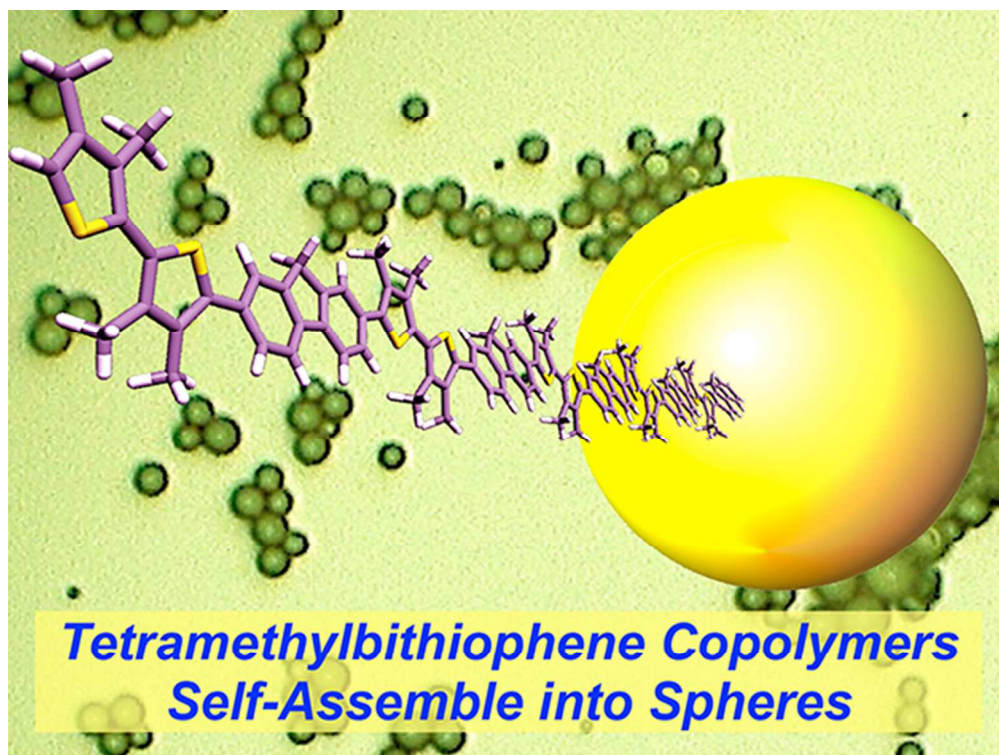
## Author addresses and notes

- <sup>a</sup> Division of Materials Science and Tsukuba Research Center for Interdisciplinary Materials Science (TIMS), Faculty of Pure and Applied Sciences, University of Tsukuba, 1-1-1 Tennodai, Tsukuba, Ibaraki 305-8573, Japan. Fax: +81 29 853 4490; Tel: +81 29 853 5030; E-mail: yamamoto@ims.tsukuba.ac.jp
- <sup>b</sup> Biomedical Research Institute, National Institute of Advanced Industrial Science and Technology (AIST), Tsukuba Central-6, 1-1-1 Higashi, Tsukuba, Ibaraki 305-8566, Japan.
- <sup>c</sup> Department of Applied Chemistry, Graduate School of Engineering, Osaka University, 2-1 Yamadaoka, Suita, Osaka 565-0871, Japan.
- <sup>d</sup> Applied Photonic Materials Group, National Institute for Materials Science (NIMS), 1-2-1, Sengen, Tsukuba, Ibaraki 305-0047, Japan.
- † Electronic Supplementary Information (ESI) available: SEM, PL spectra, FP-TRMC profiles. See DOI: 10.1039/b000000x/
- ‡ Molecular geometries were optimized by B3LYP/6–31G level DFT calculations with Gaussian09 (see ESI, ref S2†).

## References

- W. T. Ford, R. Chandran and H. Turk, *Pure Appl. Chem.* 1988, **60**, 395.

- 2 C.-W. Chen, M.-Q. Chen, T. Serizawa and M. Akashi, *Chem. Commun.* 1998, 831.
- 3 K. Suzuki, T. Yumura, M. Mizuguchi, Y. Tanaka, C.-W. Chen and M. Akashi, *J. Appl. Polym. Sci.* 2000, **77**, 2678.
- 5 4 S. Zhang, L. Chen, S. Zhou, D. Zhao and L. Wu, *Chem. Mater.* 2010, **22**, 3433.
- 5 K. Kataoka, A. Harada and Y. Nagasaki, *Adv. Drug Deliv. Rev.* 2001, **47**, 113.
- 6 H. Otsuka, Y. Nagasaki and K. Kataoka, *Adv. Drug Deliv. Rev.* 2003, **55**, 403.
- 10 7 N. Nishiyama and K. Kataoka, *Pharmacol. Ther.* 2006, **112**, 630.
- 8 O. D. Velev and E. W. Kaler, *Langmuir* 1999, **15**, 3693.
- 9 P. Techawanitchai, K. Yamamoto, M. Ebara and T. Aoyagi, *Sci. Technol. Adv. Mater.* 2011, **12**, 044609.
- 15 10 U. Lange, N. V. Roznyatovskaya and V. M. Mirsky, *Anal. Chim. Acta* 2008, **614**, 1.
- 11 Rajesh, T. Ahuja and D. Kumar, *Sens. Actuators, B* 2009, **136**, 275.
- 12 C. Wu, C. Szymanski, Z. Cain and J. McNeill, *J. Am. Chem. Soc.* 2007, **129**, 12904.
- 20 13 L. Feng, C. Zhu, H. Yuan, L. Liu, F. Lv and S. Wang, *Chem. Soc. Rev.* 2013, **42**, 6620.
- 14 J. Pecher and S. Mecking, *Chem. Rev.* 2010, **110**, 6260.
- 15 A. J. C. Kuehne, M. C. Gather and J. Sprakel, *Nat. Commun.* 2012, **3**, 1088.
- 25 16 N. Anwar, T. Willms, B. Grimme and A. J. C. Kuehne, *ACS Macro Lett.* 2013, **2**, 766.
- 17 H. Fudouji, *Sci. Tech. Adv. Mater.* 2011, **12**, 064704.
- 18 J. F. Galisteo-López, M. Ibisate, R. Sapienza, L. S. Froufe-Pérez, Á. Blanco and C. López, *Adv. Mater.* 2011, **23**, 30.
- 30 19 S. Furumi, *Polym. J.* 2013, **45**, 579.
- 20 T. Adachi, L. Tong, J. Kuwabara, T. Kanbara, A. Saeki, S. Seki and Y. Yamamoto, *J. Am. Chem. Soc.* 2013, **135**, 870.
- 21 Y. Fujinami, J. Kuwabara, W. Lu, H. Hayashi and T. Kanbara, *ACS Macro Lett.* 2012, **1**, 67.
- 35 22 J. Kuwabara, Y. Nohara, S. J. Choi, Y. Fujinami, W. Lu, K. Yoshimura, J. Oguma, K. Suenobu and T. Kanbara, *Polym. Chem.* 2013, **4**, 947.
- 23 C. Cheng, C. Yu, Y. Guo, H. Chen, Y. Feng, G. Yu and Y. Liu, *Chem. Commun.* 2013, **49**, 1998.
- 40 24 C. B. Nielsen, M. Turbics and I. McCulloch, *Adv. Mater.* 2013, **25**, 1859.
- 25 Y. Yamamoto, G. Zhang, W. Jin, T. Fukushima, N. Ishii, A. Saeki, S. Seki, S. Tagawa, T. Minari, K. Tsukagoshi and T. Aida, *Proc. Natl. Acad. Sci. USA*, 2009, **106**, 21051.
- 45 26 A. Saeki, Y. Yamamoto, Y. Koizumi, T. Fukushima, T. Aida and S. Seki, *J. Phys. Chem. Lett.* 2011, **2**, 2549.
- 27 K. Yoshino, S. Tatsuhara, Y. Kawagishi, M. Ozaki and A. A. Zakhidov, *Appl. Phys. Lett.* 1999, **74**, 2590.
- 28 A. Saeki, S. Seki, T. Takenobu, Y. Iwasa and S. Tagawa, *Adv. Mater.* 2008, **20**, 920.
- 50



53x39mm (300 x 300 DPI)